The Mechanism of Hydrogen Gas Evolution on GaAs Cathodes Elucidated by In Situ Infrared Spectroscopy

B. H. Erné,* F. Ozanam, and J.-N. Chazalviel

Laboratoire P.M.C. (U.M.R. 7643 du C.N.R.S.), École Polytechnique, 91128 Palaiseau, France

Received: December 16, 1998

The microscopic mechanism of hydrogen gas evolution on GaAs(100) cathodes is elucidated by studying the reaction intermediate, adsorbed hydrogen, using in situ infrared spectroscopy in real time. The spectra show that hydrogen adsorbs cathodically at arsenic sites only and replaces As−OH groups present in the anodic range. Absolute submonolayer coverages by adsorbed hydrogen and variations in surface dipole potential due to hydrogen adsorption are both determined quantitatively. Molecular hydrogen is formed upon proton reduction at As−H sites. The microscopic reaction mechanism at GaAs is found to be pH-independent; the reason is that rate-limiting electron transfer is not to solution species but to As−H surface sites. A simple mechanistic model accounts for the infrared spectroscopic results as well as for the electrochemistry, explaining both the approximately linear potential dependence of hydrogen surface coverage and the hysteresis loop in cyclic voltammograms.

1. Introduction

Hydrogen adsorbed at the surface of solids plays an important role in different fields of surface and materials science. It diffuses into the materials, causing embrittlement and, in the case of semiconductors, lowering conductivity by orders of magnitude.[1−4] It affects surface electrical properties, for instance leading to record low surface recombination rates of photocarriers at silicon surfaces.[5] At the surface of heterogeneous catalysts, it is a reaction intermediate in various commercially important reactions. Here, we examine its role in the cathodic production of hydrogen gas, a promising fuel for the chemical storage of energy. In this reaction, two electrons are transferred from a metal or semiconductor electrode to two aqueously solvated protons $H^+_{(aq)}$, yielding a hydrogen gas molecule $H_{2(g)}$; a hydrogen atom is temporarily adsorbed after transfer of the first electron. The fraction of the surface covered by adsorbed hydrogen is determined kinetically, by the relative rates of adsorption and desorption. With n-type gallium arsenide, we present the first quantitative and dynamic study of hydrogen adsorption at a solid−liquid interface by in situ infrared spectroscopy in real time.

The in situ spectroscopic detection of hydrogen adsorbed at electrode surfaces is based on the resonant vibrational absorption of hydrogen-to-surface bonds. Despite considerable experimental difficulties, a few authors reported infrared absorption by hydrogen adsorbed on platinum cathodes, although some controversy exists concerning peak assignments.[6−10] Surface hydrogen is more conveniently detected at attenuated-total-internal-reflection prisms of semiconducting electrodes such as GaAs,[11] and this is done here. Signals are weak even in this geometry, infrared absorption of the solution being stronger than that of a submonolayer amount of surface hydrogen by more than 3 orders of magnitude.

Until now, little was known concerning hydrogen adsorption on GaAs electrodes. It had been verified that cathodic hydrogen gas evolution requires two conduction band electrons per H_2 molecule,[12] and some transient photocurrents had been ascribed to oxidation of surface hydrogen.[13] Electroluminescence measurements by Uosaki et al.[14] gave strong indirect evidence for the existence of adsorbed hydrogen as an intermediate in the hydrogen evolution reaction, but direct proof had not yet been reported. By in situ spectroscopic ellipsometry, we demonstrated that surface hydrogen destabilizes the surface, a small percentage of the cathodic current leading to the formation of metallic gallium as soon as the potential is more negative than the Ga^0/Ga^{3+} redox potential.[11] The formation of metallic gallium, whose presence is easily detected by in situ infrared spectroscopy too, will generally be avoided in this paper by not going more negative than that potential. Under such conditions, the surface is thought to be rough and arsenic rich, since gallium is preferentially dissolved.[11] In the present paper, which expands upon a recent brief report,[15] we focus on hydrogen adsorption and hydrogen gas evolution at such surfaces.

The cathodic hydrogen gas evolution reaction has been used since the beginning of the 20th century as a model system for the study of electrode kinetics. This is due in part to the simplicity of the reaction: with metal electrodes, even indirect information such as the slope of current−potential curves can be interpreted as an indication for a precise mechanism.[16] This and many other multiple-step reactions in electrochemistry are assumed to proceed via surface intermediates, but rarely have such intermediates been observed by direct methods. Here, with n-GaAs electrodes, we detect cathodic surface hydrogen spectroscopically, and we determine its concentration quantitatively, the first time this is done for any electrode material using in situ infrared spectroscopy. The effect of hydrogen coverage on interfacial potential distribution is a key element for the understanding of the current−potential characteristics and will be investigated using an original transient flatband potential measurement technique. After some experimental details, the results will be presented. They include time-resolved potential-dependent measurements of surface coverage by hydrogen and surface free-electron concentration. Then, a highly detailed

* Corresponding author.

10.1021/jp984765t CCC: $18.00
Published on Web 03/27/1999

picture is drawn of the microscopic reaction mechanism of hydrogen gas evolution on GaAs cathodes. A reaction model is developed, and it is tested by comparing simulated electrochemical behavior with experiment.

2. Experimental Section

The experiments were performed on ⟨100⟩-oriented n-GaAs single crystals grown by the liquid encapsulated Czochralski method and purchased from MCP Wafer Technology, U.K. ($N_D = 8 \times 10^{15}$ cm^{-3}) and from the Institute of Electronic Materials Technology, Poland ($N_D = 4 \times 10^{15}$ and 7×10^{16} cm^{-3}). Two-side polished 500 μm thick wafers were used to make multiple-total-internal-reflection prisms. Ohmic contacts were obtained by evaporating gold (+10% germanium) under reduced pressure (10^{-3} Pa) while the sample was being cooled from 400 °C down to room temperature. The surface was pretreated with concentrated HCl in order to remove oxides and according to a recipe by Aspnes and Studna[17] for obtaining ellipsometrically clean GaAs surfaces. On the basis of our previous results, the GaAs surface is probably OH-covered after such a treatment.[15]

The electrochemical cell is described in ref 18, with the vertically oriented prismatic GaAs electrode (45° angles) exposing an area of 0.8 cm^2 to a circulating aqueous solution of HCl or NaOH. The cell includes a platinum counter electrode and an Ag/AgCl in saturated KCl reference electrode. The circulation rate was sufficiently high that no hydrogen bubbles were detected at the surface during the experiments reported here (when a bubble is present, this causes a strong decrease in infrared absorbance by the electrolyte solution). When needed, illumination was achieved using a white light source. The experiments were carried out at room temperature on a short time scale, so that diffusion of hydrogen into GaAs can be neglected.

The aqueous oxygen concentration was kept minimal except when otherwise indicated. The solution was purged using a flow of nitrogen from which traces of oxygen were removed by bubbling in a chromous chloride solution ($CrCl_2$). The solution was purged in a separate compartment before it was brought into contact with GaAs, to limit GaAs surface damage due to reaction with residual oxygen. During the electrochemical measurements, a nitrogen flow continued to purge the electrolyte solution and simultaneously ensured solution circulation. The counter electrode, at which oxygen is produced during cathodic polarization of GaAs, was placed in another separate compartment, connected to the rest of the cell via a salt bridge.

Infrared absorbance was measured with a Bomem MB 100 Fourier transform infrared spectrometer set at a nominal resolution of 4 cm^{-1}. The absorbance at wave number σ is defined as $(1/N)\ \ln[I^\sigma(U_0)/I^\sigma(U)]$, where $N \approx 10$ is the number of useful reflections at the electrochemical interface, $I^\sigma(U)$ is the light intensity at wave number σ reaching the detector at potential U, and $I^\sigma(U_0)$ the same but under reference conditions at potential U_0. Spectra were recorded in the dark, unless otherwise specified. During dynamic measurements of surface hydrogen concentration, infrared absorbance was recorded continuously; the integration time is therefore given by the distance between two experimental points in a figure.

Changes in flatband potential were monitored by interrupting the cyclic potential scans or other experiments every 100 ms for a 1 ms period and stepping the potential to various positive potentials, at which the differential capacitance of the semiconductor space charge layer was measured (for details on the setup, see ref 19).

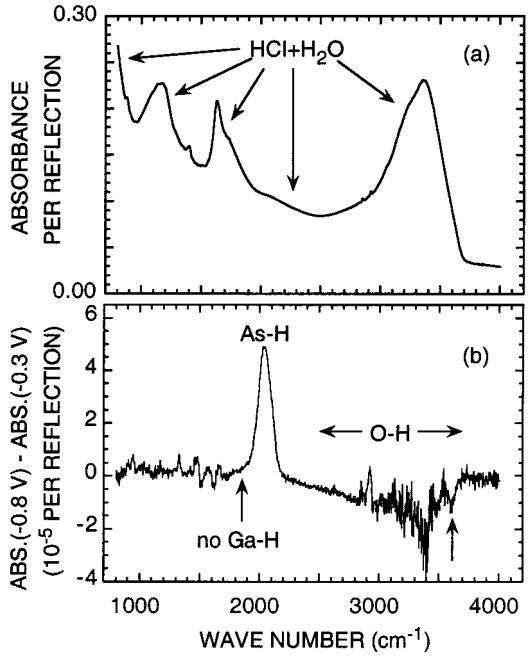

Figure 1. (a) Total infrared absorbance of the n-GaAs/6 M $HCl_{(aq)}$ interface (reference: the n-GaAs/N_2 interface); (b) change in infrared absorbance when the applied potential is changed from −0.3 to −0.8 V vs Ag/AgCl (average of 1500 cycles; for each cycle, potential was set to −0.8 V during 4 s and to −0.3 V during 8 s; spectra recorded under white light illumination with an intensity corresponding to an anodic photocurrent density of 100 μA cm^{-2}).

3. Results

The results are presented in four parts. First, the adsorption site of hydrogen at the surface of GaAs cathodes is characterized. Second, a coulometric titration of surface hydrogen is performed in order to determine the surface concentration of adsorbed hydrogen quantitatively. Third, the transient capacitance measurement technique is introduced. And fourth, surface hydrogen coverage and interfacial capacitance are measured in real time during cyclic potential scans.

3.1. Spectroscopic Characterization of Surface Hydrogen. Figure 1a shows the total infrared absorbance of the n-GaAs/$HCl_{(aq)}$ interface. The spectrum is completely dominated by the absorbance of the solution probed by the evanescent wave (probing depth ≈ 0.5 μm at 1000 cm^{-1}). For instance, O−H stretch vibrations are seen in the 3000−3500 cm^{-1} range and H−O−H bending modes around 1650 cm^{-1}. To reveal the presence of surface species, measurements are performed in the potential difference mode. In this way, constant contributions to the absorbance are eliminated.

Figure 1b presents the change in interfacial infrared absorbance as a result of going from the potential where no current is measured in the steady state (−0.3 V vs Ag/AgCl) to a potential where hydrogen evolution occurs (−0.8 V vs Ag/AgCl). Absorbance increases at 2050 cm^{-1} and decreases in the 2500−3700 cm^{-1} range. Comparison with the literature indicates that the absorbance at 2050 cm^{-1} corresponds to As−H bonds only; no Ga−H absorption is found, even when the potential is set to a value where metallic gallium is present at the surface. In contrast, spectra of hydrogen adsorbed on GaAs-(100) from the gas phase show absorption both by As−H and Ga−H.[20,21] The nearly symmetric line shape suggests that monohydride species are the dominant species. The broadness of the signal may be accounted for in terms of interaction between As−H and water (see ref 22 for the analogous case of

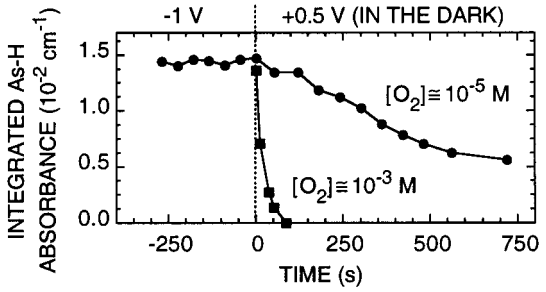

Figure 2. Evolution of As−H coverage at the n-GaAs surface in 1 M HCl, after stepping potential from −1 to +0.5 V vs Ag/AgCl in the dark, for two different concentrations of dissolved oxygen.

Si−H) and/or by the existence of distinct As−H sites at the surface. We ascribe the absorbance decrease in the 2500−3700 cm^{-1} range to loss of surface OH-groups, present at the surface in the anodic range and replaced by adsorbed hydrogen in the cathodic range. The signal might arise either from surface OH-groups or from H_2O molecules; however, changes in water absorption by O−H stretch vibrations would have occurred over a narrower range and would have given rise to a stronger signal in the 1650 cm^{-1} range (compare with Figure 1a). Furthermore, the separate peak at 3600 cm^{-1} evokes absorption by isolated OH-groups not hydrogen bonded to other OH-groups, which leads to the ascription of the broad signal to AsO−H. Several weak vibrational features are also detected near 1450, 1700, and 2900 cm^{-1}; these are artifacts ascribed to imperfect cancellation of O-ring seal absorption. Absorption by As−O bonds falls outside our spectral window. Peak assignments were verified by measurements in deuterated solutions, in which the signals shift to wave numbers lower by a factor $\approx \sqrt{2}$, due to the higher reduced mass of the oscillators.[11] Moreover, the As−H bonds were found to absorb *p*-polarized light more strongly than *s*-polarized light,[11] confirming that they are at the surface rather than inside the solid. Absorbance by As−H is found at the same wave numbers in acidic and alkaline solutions.

3.2. Absolute Surface Concentration of Hydrogen. Qualitatively, we already showed in another paper that the surface concentration of hydrogen adsorbed on GaAs cathodes depends more or less linearly on the applied potential.[11] Measurements of the anodic charge required to convert a cathodic GaAs surface into an anodic surface suggest that the absolute surface coverages are of the order of a monolayer.[13,23,24] Here, in situ infrared spectroscopy and anodic charge measurements are combined in order to determine absolute hydrogen surface concentrations quantitatively.

A coulometric titration of the surface hydrogen observed by in situ infrared spectroscopy can be carried out using anodic current, provided that the dissolved oxygen concentration is sufficiently low. Indeed, time-resolved measurements reveal that the disappearance of cathodically adsorbed hydrogen at positive potentials is due only to anodic reaction with holes (negligible in the dark, when the current density j was ≈20 nA cm^{-2} for $N_D \approx 10^{16}$ cm^{-3}) and chemical reaction with dissolved oxidizing agents (e.g., oxygen, see Figure 2). After measurement of the As−H absorbance under cathodic conditions, the potential was changed to the steady-state rest potential under illumination. Just after the jump, a photocurrent appeared and decreased to zero as surface hydrogen was removed (Figure 3). It is well-known that no electrochemical dissolution of n-GaAs occurs at this potential in indifferent electrolyte solution; a photogenerated hole is much more likely to recombine with an electron than to oxidize a GaAs bond under those conditions.[25,26] Our measurements show that when As−H bonds are present at the surface,

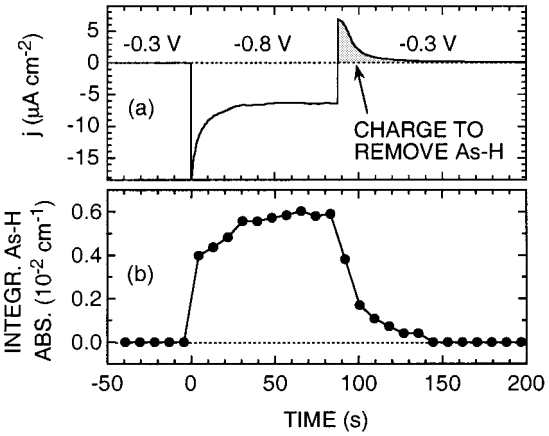

Figure 3. Changes in (a) current density and (b) As−H absorbance of illuminated n-GaAs electrodes in 1 M HCl upon stepping potential from −0.3 to −0.8 V vs Ag/AgCl and back (white light illumination with an intensity corresponding to the maximum anodic current density seen in the figure).

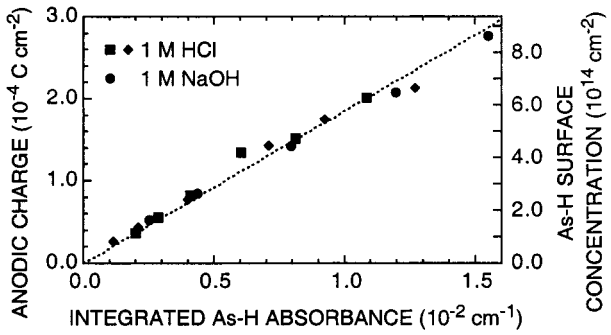

Figure 4. Anodic charge required to remove hydrogen from n-GaAs surfaces in 1 M HCl or 1 M NaOH as a function of the change in As−H absorbance (different symbols refer to different electrodes). These coulometric measurements provide an absolute calibration of the As−H surface concentration (right-hand scale).

their oxidation by photogenerated holes is kinetically even more favorable than recombination with electrons, hence a transient photoanodic current is observed at this potential due to oxidation of surface hydrogen. The anodic charge measured by integrating the transient photocurrent is proportional to the initial As−H absorbance (Figure 4). In HCl solutions, polarization was kept brief (a few seconds) at potentials $U < -0.8$ V vs Ag/AgCl ($U < -1.6$ V in NaOH solutions), to limit the formation of metallic gallium, which represents a few percent of the cathodic current at those potentials.[11] The proportionality is strong evidence that the anodic charge is used almost exclusively for the oxidation of surface hydrogen. This is no longer the case when polarization in the stability range of metallic gallium is carried out for longer periods, because the anodic charge required to oxidize the surface then includes a sizable contribution due to the oxidation of metallic gallium. The same proportionality constant is found in acidic and alkaline solutions with different GaAs samples and light intensities. On the assumption, suggested by Figure 1b, that all As−H is oxidized to As−OH, requiring two holes per As−H, integrated absorbances by surface As−H can be converted to absolute surface coverage using Figure 4. The integrated absorbance when all 6.26×10^{14} cm^{-2} arsenic atoms in a (100) plane are bound to a hydrogen atom is apparently 1.08×10^{-2} cm^{-1} per reflection. This value seems quite reasonable when compared with the absorbance of surface hydrogen in other systems under conditions where surface coverage appears to be maximal.[20,21,27−29]

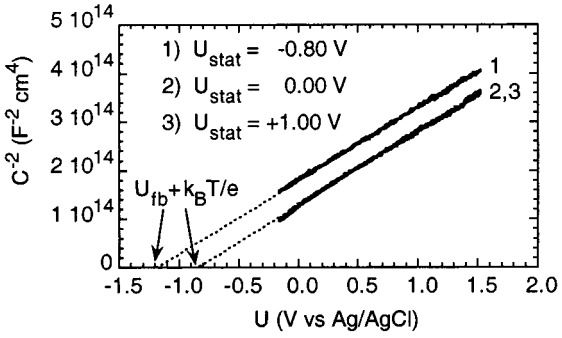

Figure 5. Transient capacitance of the n-GaAs/1 M HCl interface in the dark plotted according to the Mott−Schottky relation (eq 1) for different stationary potentials U_{stat}. Every 100 ms, the potential was switched from U_{stat} to U for a 1 ms period during which the differential capacitance was measured; U was scanned at 50 mV s^{-1} ($N_D \approx 7 \times 10^{16}$ cm^{-3}). The extrapolated flatband potential U_{fb} is seen to depend on U_{stat}.

3.3. The Transient Capacitance Measurement Technique. In an earlier paper,[11] it was concluded that hydrogen adsorption on GaAs cathodes probably causes a change of the surface dipole potential. In the present work, to quantify such changes, in situ infrared measurements are performed simultaneously with transient measurements of the interfacial capacitance. This section illustrates how the transient capacitance measurement technique[19] allows the rapid determination (in a millisecond or less) of the flatband potential corresponding to a short-lived surface chemical composition.

The electrode capacitance under depletion conditions is determined by the capacitance C_{sc} of the semiconductor space charge layer. Therefore, its dependence on the applied potential U obeys the Mott−Schottky relation:[30]

$$C_{sc}^{-2} = 2\,(e\epsilon\epsilon_0 N_D)^{-1}\,(U - U_{fb} - k_B T/e) \qquad (1)$$

where e is the positive elementary charge, ϵ the dielectric constant of GaAs,[30] ϵ_0 the permittivity of vacuum, U_{fb} the flatband potential, k_B the Boltzmann constant, and T the absolute temperature. Changes of the surface dipole potential are revealed by changes of the flatband potential value obtained by extrapolating a plot of C^{2-} versus U to $C^{-2} = 0$.

Figure 5 presents the Mott−Schottky plots for n-GaAs(100) electrodes in 1 M HCl having reached a steady-state chemical surface composition at +1, 0, and −0.8 V vs Ag/AgCl. Every 100 ms, the stationary potential U_{stat} was left for a period of 1 ms during which the differential capacitance was measured at potentials scanned in the anodic range. The transient Mott−Schottky plots are the same for stationary potentials of +1 and 0 V, indicating that the surface dipole potential does not change. When the Mott−Schottky plot is measured in a more classical way, i.e., the stationary potential and the potential at which the capacitance measurements are carried out are the same, points are obtained which fall on the same curve. In contrast, the flatband potential corresponding to an electrode polarized at −0.8 V is significantly more negative, in agreement with rapidly measured Mott−Schottky plots reported by others.[31,32] The transient capacitance technique makes it possible to monitor flatband potential changes in real time during electrochemical surface treatments. For example, the measurement of cyclic voltammograms can be interrupted every 100 ms in order to check the flatband potential by a 1 ms measurement of the capacitance at a potential where the Mott−Schottky plot is linear.

Simultaneous infrared and capacitance measurements were performed only on samples with a dopant density of 7×10^{16} cm^{-3}. In situ infrared measurements are more conveniently carried out on less doped samples, because free electrons absorb infrared light over the entire spectral range,[33] and the transmitted light intensity decreases exponentially with dopant density. However, at low dopant densities, capacitance measurements are seriously affected by deep electronic centers in the band gap generally present at a concentration of $\approx 10^{16}$ cm^{-3}, so-called EL2 centers.[1,30,34,35] Hysteresis effects occur, because whereas these levels gain electrons easily when the Fermi level is sufficiently high, the reverse process, electron loss, is extremely slow, occurring on a time scale of seconds at room temperature. At a dopant density of 7×10^{16} cm^{-3}, these undesired effects are negligible and infrared transmittance is not yet prohibitively low.

3.4. Dynamic Potential Dependence of j, θ_H, and U_{fb}. Simultaneous dynamic measurements of the current density j, the hydrogen surface coverage θ_H, and the flatband potential U_{fb} were carried out on n-GaAs electrodes under illumination and in the dark.

Under illumination, the hydrogen surface coverage was monitored during cyclic potential scans in 1 M HCl solution at two different scan rates. Current density is shown in Figure 6a, hydrogen surface coverage in Figure 6b, and flatband potential in Figure 6c. The 0.5 mV s^{-1} scan approximates steady-state conditions, while the 50 mV s^{-1} scan illustrates the system dynamics.

The n-GaAs electrochemical interface is a rectifying contact, much like a Schottky diode. Under forward bias, cathodic current density due to hydrogen gas evolution changes exponentially with the applied potential, while hydrogen surface coverage changes more or less linearly. Under reverse bias, the anodic current density is very low in the dark and corresponds to one hole per absorbed photon under illumination.[25,26] In the steady state, anodic current causes dissolution of the semiconductor,[25,26] while in the 50 mV s^{-1} scan in Figure 6, as long as As−H is present, it can be shown using the coulometric titration in Figure 4 that all the anodic current is consumed for the oxidation of surface hydrogen.

One important difference with a Schottky diode is that the applied potential drops partly across the semiconductor space charge layer and partly on the electrolyte side of the interface.[25,26] In Figure 6c, changes in potential drop on the electrolyte side of the interface are revealed by changes in the flatband potential. In the reverse bias range, U_{fb} is about −0.85 V in the dark and somewhat more positive under illumination, due to the positive charge of dissolution intermediates.[32,36−38] Under forward bias, U_{fb} shifts negatively, in agreement with steady-state measurements by Uhlendorf et al.[39] Our dynamic measurements clearly indicate that the position of U_{fb} is correlated to the hydrogen surface coverage. U_{fb} and hydrogen surface coverage exhibit approximately the same hysteresis, about 200 mV during the 0.5 mV s^{-1} scan and significantly more during the 50 mV s^{-1} scan. During the negative scans, first the positive surface charge disappears, and then, an additional negative U_{fb} shift of about 50 mV occurs per 10^{14} cm^{-2} As−H bonds. During the positive scans, first As−H disappears, after which positive surface charge reappears, both causing positive shift of U_{fb}. This is the first direct evidence in electrochemistry that a change from OH- to H-surface coverage causes a change in the surface dipole potential.

In the dark, the relationship between hydrogen surface coverage and surface dipole potential was investigated further.

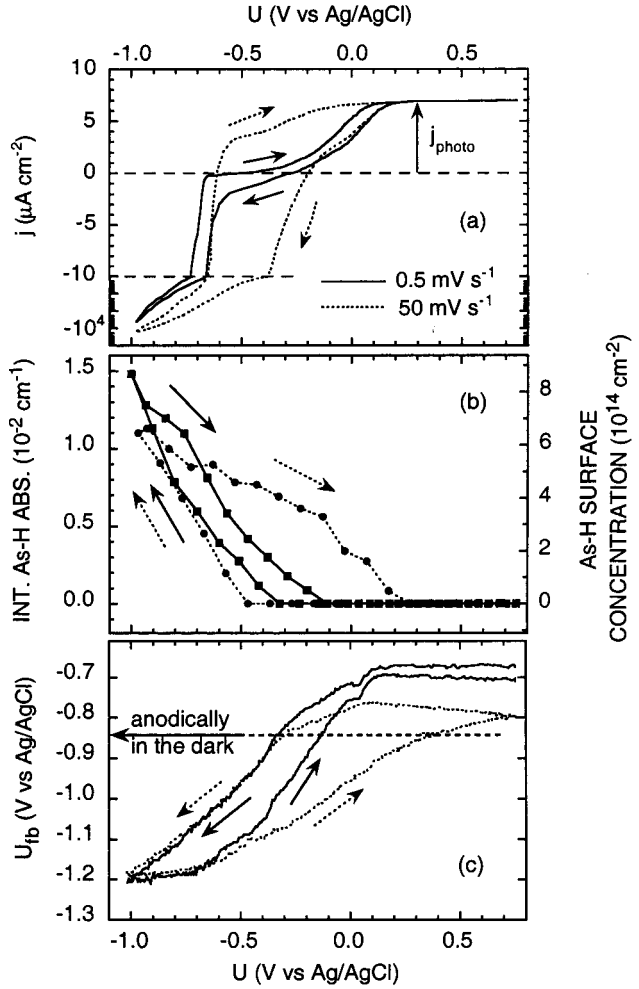

Figure 6. (a) Current density, (b) surface coverage by hydrogen (determined by infrared measurements, according to the calibration in Figure 4 and for a reference potential of +0.5 V vs Ag/AgCl under steady-state conditions), and (c) flatband potential (determined as in Figure 5) of illuminated n-GaAs electrodes in 1 M HCl monitored during cyclic potential scans at two different scan rates (same light intensity as for Figure 3).

First, the effect of hydrogen adsorption on the surface dipole potential was corroborated by the following experiment. The surface was hydrogenated in the cathodic range, after which θ_H and U_{fb} were monitored during chemical dehydrogenation by residual oxygen in the anodic range (Figure 7). U_{fb} required approximately the same amount of time to reach a new steady state as θ_H did to drop to zero, demonstrating that the two are correlated. The process was more rapid when the electrolyte solution was circulated than when it was not, because circulation accelerated chemical oxidation of surface hydrogen by increasing the rate at which dissolved oxygen was brought to the surface. The current density is stationary at +50 nA cm^{-2} soon after +0.50 V is applied. The disappearance of As−H is purely chemical and does not involve electron injection, because the disappearance of 6×10^{14} cm^{-2} As−H bonds during the first 100 s would have corresponded to a much higher average current density of about +1 μA cm^{-2}.

In the dark, current density, θ_H, and U_{fb} were also monitored during cyclic potential scans at pH 0 and pH 14 (Figure 8). The current density and θ_H curves at pH 14 are shifted negatively by about 800 mV with respect to those at pH 0. In the reverse bias range, the flatband potential is shifted by the same amount. The current−potential curves and the changes in θ_H and U_{fb} which occur during cathodic polarization are very

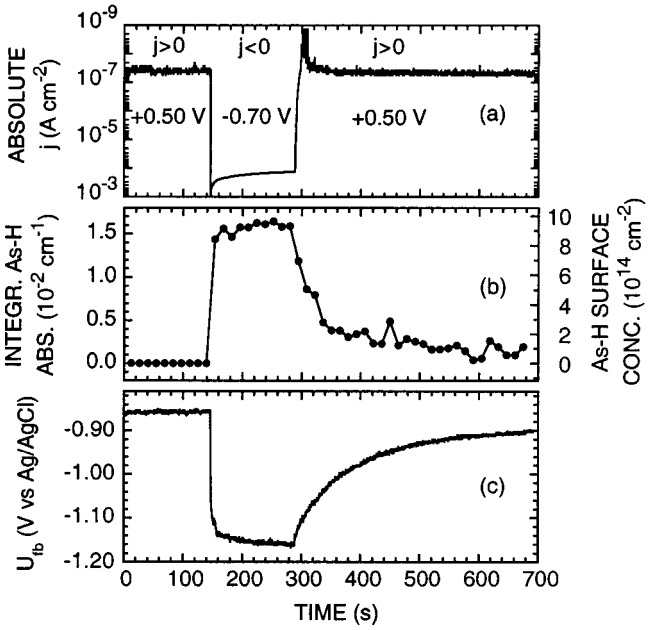

Figure 7. Changes in (a) current density, (b) As−H absorbance (surface concentration according to calibration in Figure 4, reference potential +0.5 V vs Ag/AgCl), and (c) flatband potential (determined as in Figure 5) of n-GaAs electrodes in the dark in 1 M HCl upon stepping potential from +0.5 to −0.7 V vs Ag/AgCl and back. Notice the close correlation between the variations in As−H absorbance and U_{fb}.

similar at pH 0 and pH 14, although at a same current density, θ_H values are higher at pH 14 by a factor of about two. At potentials where hydrogen evolution occurs, θ_H and U_{fb} were found to be practically the same in the dark and under illumination.

The scans presented by full lines in Figure 8 were not measured on freshly polished electrodes but rather after two or three preliminary scans. This pretreatment ensured that subsequent consecutive scans were practically the same, so that irreversible changes occurring during a single scan could be neglected. The first scans on a polished electrode give lower current densities at potentials where hydrogen evolution occurs; however, the potential dependences of θ_H and U_{fb} are practically the same (see the dotted lines in Figure 8).

The oxygen concentration has a significant effect on the current density at which As−H first appears in the dark during potential scans in the negative direction. In an oxygen-saturated solution, no As−H is observed before $j \approx -100$ μA cm^{-2}, while As−H first appears at much lower j in purged solutions, at $j \approx -1$ μA cm^{-2} in Figure 8. At potentials positive of those at which As−H is observed, the current depends on the solution circulation rate, as expected for the diffusion-limited reduction of aqueous oxidants. An oxygen concentration of 2 μM can be calculated from a diffusion-limited current density of $j \approx -1$ μA cm^{-2} (4 electrons per O_2 molecule, 200 μm diffusion layer thickness, diffusion coefficient by Kolthoff and Miller[40]), versus about 1 mM for oxygen-saturated solutions.[41,42] Oxygen can be fully removed from solution by adding an excess concentration of reductor, e.g., 0.3 M Cr^{2+} in 1 M HCl. With that solution, no cathodic current is observed before −0.36 V, but hydrogen gas evolution is difficult to study, since Cr^{3+} reduction competes with that of H^+.

After sufficient cathodic aging, scans negative of −0.8 V at pH 0 are significantly affected by the appearance of metallic gallium,[11] correlated to a positive shift of the flatband potential (Figure 9). When enough surface metallic gallium is present, the current no longer shows hysteresis between potential scans

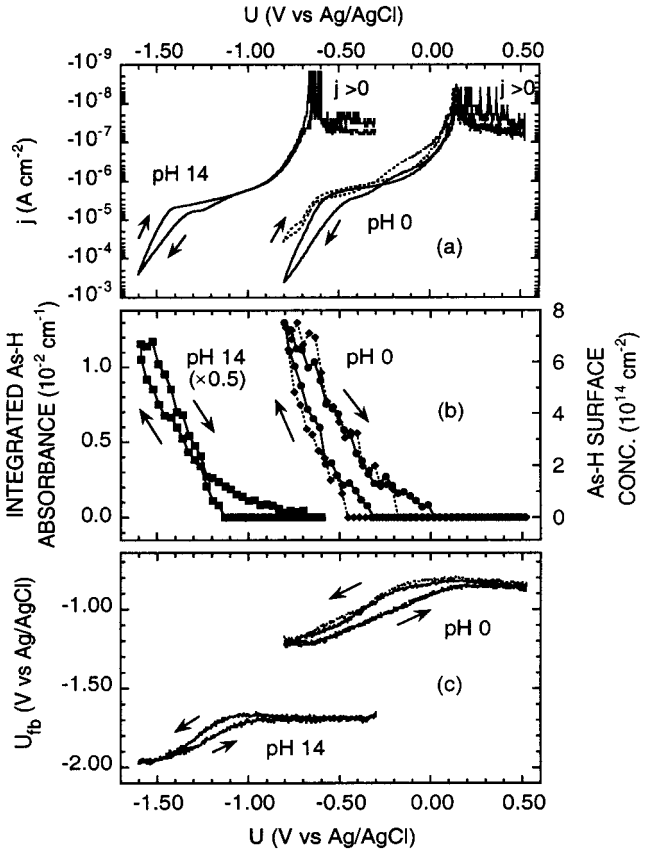

Figure 8. (a) Current density, (b) surface coverage by hydrogen according to the calibration in Figure 4 and for reference potentials of +0.5 V vs Ag/AgCl at pH 0 and −0.3 V vs Ag/AgCl at pH 14 under steady-state conditions, and (c) flatband potential (determined as in Figure 5) of cathodically pretreated n-GaAs electrodes in the dark at pH 0 (1 M HCl) and pH 14 (1 M NaOH), and monitored during cyclic potential scans at 1 mV s^{-1}. The dotted lines indicate measurements at pH 0 before cathodic pretreatment.

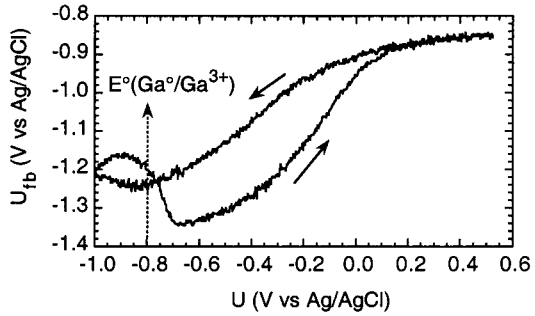

Figure 9. Flatband potential of n-GaAs electrodes in the dark in 1 M HCl monitored during cyclic potential scans at 1 mV s^{-1} to potentials where metallic gallium is formed ($U < -0.8$ V vs Ag/AgCl[11]).

in negative and in positive directions in the stability range of metallic gallium.[11]

It was verified by the infrared-active local pH probe technique[43] that surface pH remained constant during the current−potential scans in pH 0 and pH 14 solutions. This technique uses in situ infrared spectroscopy and relies on the fact that the evanescent wave penetrates only about 0.5 μm into the solution;[44] this is a very small distance compared to the diffusion layer thickness of about 200 μm calculated under our circulation conditions from a diffusion-limited current density of −4 mA cm^{-2} in 0.01 M $H^+_{(aq)}$ and from the diffusion coefficient of $H^+_{(aq)}$.[45] Phosphates were used as the infrared absorbing pH probes. From an observed constant [H_3PO_4]/[$H_2PO_4^-$] concentration ratio at pH 0 and a constant [HPO_4^{2-}]/[PO_4^{3-}] ratio at pH 14 during current−potential scans, it can be concluded that the pH at the surface is always the same as that in the bulk of the electrolyte solution during our experiments, within less than 0.1 pH unit.

4. Discussion

On the basis of the presented experimental results, a detailed picture is drawn of the microscopic mechanism of hydrogen gas evolution on GaAs cathodes. First, the structure and chemical composition of the surface are discussed, as well as the different origins of variations of the flatband potential. The most important electrochemical reaction steps are reviewed, and the rate-limiting step is identified. Finally, all the acquired information is combined in order to explain the dynamic behavior of GaAs electrodes.

4.1. Surface Structure and Chemical Composition. Differential in situ infrared spectra (e.g., Figure 1b) indicate that GaAs(100) electrode surfaces are OH-covered in the anodic range and that a large fraction of the OH-groups is replaced by adsorbed hydrogen in the cathodic range. Surface hydrogen is bound at arsenic sites only. Since replacing AsH by AsOH involves two electrons and replacing AsH by As$^\bullet$ only one electron, the equal results of the coulometric titrations at pH 0 and pH 14 (Figure 4) indicate that the anodic surface is OH-terminated in the entire pH range.

At the most negative potentials, the absolute surface hydrogen coverage exceeds 6.26×10^{14} cm^{-2}, the density of arsenic atoms at an unreconstructed GaAs(100) surface. While this might suggest the presence of arsenic dihydride, it is just as likely due to surface (micro)roughness, resulting from cathodic and anodic decomposition. We demonstrated elsewhere that a minor percentage of the cathodic current is due to decomposition reactions which cause surface roughening.[11] Considering the fact that three hydrogen atoms per arsenic atom yield arsine gas, surface roughness is obvious after prolonged cathodic polarization, when hydrogen surface coverage corresponds to more than two monolayers.[11] Surface coverage by hydrogen was not observed to stabilize at a maximum value at the most negative potentials due to experimental limitations (metallic gallium deposition and hydrogen bubble formation). In conclusion, our data indicate that AsH is the dominant surface species during hydrogen gas evolution, but it is likely that some residual coverage by AsOH is maintained even at the most negative potentials in this study.

Under vacuum conditions, surface reconstruction occurs at GaAs(100),[20] because this lowers the energy by eliminating dangling bonds. Our results explain why, in contrast, GaAs(100) surfaces at the electrolyte interface can be found unreconstructed, as was shown first by Koinuma and Uosaki[46] using atomically resolved in situ atomic force microscopy (AFM): before hydrogen is adsorbed, dangling bonds are already saturated with adsorbed OH groups. Our results suggest that the plane seen by AFM consists only of arsenic atoms. For further illustration, see the didactic picture drawn by Allongue and Cachet[47] of the first atomic planes of GaAs(100) terminated by a (1×1) arsenic face.

It is perhaps somewhat surprising that only As−H bonds are observed instead of Ga−H, considering that surface stability against (electro)chemical oxidation is known to increase in the sequence (111)As < (100) < (111)Ga.[25,26,48−50] The stability of Ga(111) against oxidation is presumably related to a lack of unpaired electrons at this face.[51,52] Since roughening processes promote a surface terminated by the most stable facets, one

would therefore expect that the bare microrough anodic surface is terminated by Ga(111) facets. The situation is different for cathodic surfaces, however. As−H bonds are much more stable than Ga−H bonds,[53,54] so that it seems plausible that cathodic polarization promotes arsenic-terminated surfaces. Bonding to OH-groups could also favor an arsenic-terminated surface: judging from the fact that all aqueous arsenic species are oxygenated while Ga^{3+} is stable at sufficiently low pH,[53,54] As−O bonds are more stable than Ga−O bonds.

The higher surface coverages by hydrogen in alkaline solutions suggest higher surface roughness than in acidic solutions. Relatively low stability of GaAs surfaces in alkaline solutions was reported before.[55] One pH-dependent change in surface chemistry could be related to the solubility of oxidized arsenic. Elemental arsenic is thermodynamically stable in deaerated solutions at any pH, but residual oxygen oxidizes arsenic, and surface oxides on elemental arsenic are orders of magnitude more soluble at pH 14 than at pH 0.[54] This would explain observations that (photo)anodic treatment yields a porous arsenic layer in acidic solution,[11,56−59] whereas elemental arsenic is removed in alkaline solution.[56,60−63] The observation of an atomically flat (100) face by AFM in 10 mM H_2SO_4 [46] demonstrates that GaAs surfaces in the dark are relatively stable in oxygen-free solutions. In oxygenated solutions of 1 to 12 M HCl, the chemical dissolution rate of GaAs is what one would expect on the basis of oxidation by dissolved oxygen.[63]

4.2. Origins of the Shifts in Flatband Potential. A change $\Delta\phi$ in the potential applied to a GaAs electrode is distributed over the semiconductor space charge layer ($\Delta\phi_{sc}$), the semiconductor surface, and the electrolyte side of the interface. Surface contributions may include those of surface states, specifically adsorbed ionic species, and dipolar species attached to the surface. Following Gerischer et al.[64] we call $\Delta\phi_{dip}$ the contribution associated with attached neutral dipoles, and we include in the Helmholtz term $\Delta\phi_H$ the other surface and electrolyte contributions:

$$\Delta\phi = \Delta\phi_{sc} + \Delta\phi_{dip} + \Delta\phi_H \quad (2)$$

In this work, the semiconductor space charge layer always remains depleted, even in the forward bias range, due to changes in potential drop on the solution side of the interface ($\Delta\phi_{dip} + \Delta\phi_H$). Those changes are observed as shifts in the extrapolated flatband potential in capacitance measurements (e.g., see Figure 5), shifts which reveal changes in $\Delta\phi_{sc}$ at constant potential:

$$\Delta\phi_{sc} = U - U_{fb} \quad (3)$$

The strongest effect on U_{fb} observed here is that of pH. Under reverse bias, U_{fb} is about 800 mV more negative at pH 14 than at pH 0 (Figure 8), in agreement with others who found that the flatband potential of GaAs electrodes shifts by 60 mV per pH unit.[65,66] The classical explanation is in terms of a pH-dependent adsorption/desorption equilibrium.[26,67,68] It has been convincingly demonstrated for GaAs that the equilibrium is chemical, i.e., it does not involve electron exchange: at fixed pH, the band positions are identical for p- and for n-type electrodes under severe depletion, when no majority carriers are present at the surface.[67,68] Here, the equilibrium probably involves the dissociation of surface hydroxyl groups bound to arsenic atoms of GaAs:

$$AsOH \rightleftarrows AsO^- + H^+_{(aq)} \quad (4)$$

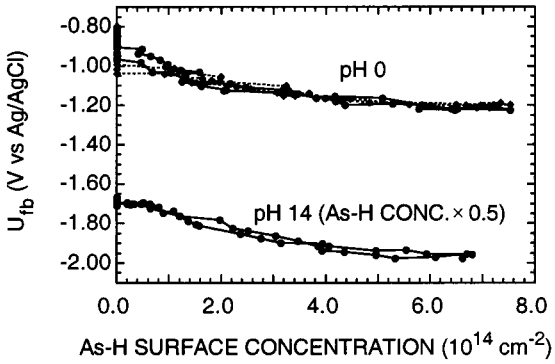

Figure 10. Flatband potential plotted against surface hydrogen coverage (same data as Figure 8).

Shifts in flatband potential as a result of pH changes are then due to changes in the surface coverage θ_{AsO^-} by the negatively charged AsO^-. A contribution $-eN_s\theta_{AsO^-}$ to the surface charge density Q_s, where N_s is the total density of surface sites, affects the potential drop across the Helmholtz layer by $\Delta\phi_H$ (and therefore also U_{fb}) according to

$$\Delta\phi_H = Q_s/C_H \quad (5)$$

where C_H is the capacitance of the Helmholtz layer. The effect of pH on U_{fb} can be calculated on the assumption that eq 4 represents a thermodynamic equilibrium and that the activities of surface species are proportional to their surface coverages (see also refs 69,70):

$$\Delta\phi_H = -eN_s\theta_{AsO^-}/C_H = -\frac{k_BT}{e}\ln(10)\,\mathrm{pH} + \frac{k_BT}{e}\ln\left(\frac{-\Delta\phi_H C_H}{eN_s}\right) - \frac{k_BT}{e}\ln(\theta_{AsOH}) + \text{constant} \quad (6)$$

Closer examination of the various terms shows that variations of $\Delta\phi_H$ are dominated by the first term of the right-hand member: $-\Delta\phi_H$ varies by 60 mV [$\approx (k_BT/e)\ln(10)$] per pH unit at room temperature. Surface coverage by AsO^- adjusts itself to a small value proportional to the pH.

Charged electrochemical reaction intermediates can also cause a shift in U_{fb} to an extent given by eq 5. It is well-known that during photoanodic dissolution of n-GaAs, positively charged surface intermediates cause a positive shift of U_{fb}.[32,36−38] With some materials, charged electrochemical reaction intermediates are even responsible for the pH dependence of U_{fb}.[71,72] Here, surface coverage by negatively charged intermediates in the hydrogen evolution reaction is very low, because they are rapidly neutralized by protons, as will be discussed later. Evidence that surface negative charge can be neglected is given in Figure 7, in which the U_{fb} transient at open circuit appears to be correlated only to hydrogen surface coverage—no rapid part is present due to the disappearance of surface charge. The rate at which j attains the stationary reverse bias value (Figure 7a) suggests that cathodic surface charge is at most a small fraction of a microcoulomb per square centimeter.

Figure 7 indicates that surface hydrogen can maintain U_{fb} at more negative values than when no surface hydrogen is present even when almost no current is flowing. This can be explained in terms of the earlier conclusion that As−H dipoles replace As−OH dipoles, causing a change of the potential drop across the layer of surface dipoles. Figure 10 gives the flatband

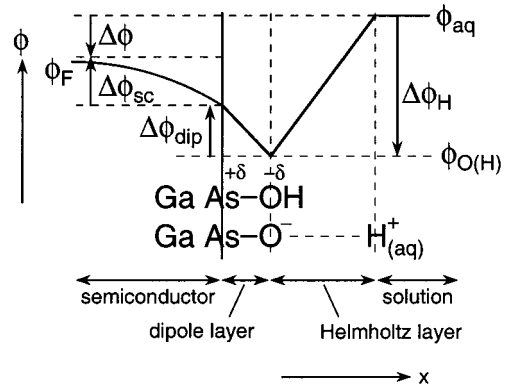

Figure 11. Spatial distribution of the electrostatic potential $\phi(x)$ at the n-GaAs/aqueous solution interface. Changes $\Delta\phi$ in the potential difference between semiconductor (ϕ_F) and solution (ϕ_{aq}) fall partially across the semiconductor space−charge layer ($\Delta\phi_{sc}$), the adsorbed dipole layer ($\Delta\phi_{dip}$), and the Helmholtz layer ($\Delta\phi_H$).

potential as a function of hydrogen surface coverage. The same data were presented as a function of the applied potential in Figure 8, in which both U_{fb} and θ_H showed considerable hysteresis. The lack of hysteresis in Figure 10 demonstrates that one hydrogen surface coverage corresponds to only one potential drop across the surface dipole layer. No other U_{fb} shift is observed than that correlated to hydrogen surface coverage. The change in dipolar potential drop ϕ_{dip} is not completely linear with the dipole surface coverages, and several partial explanations can be proposed for this. First, interfacial charge in AsO^- changes with AsOH coverage, especially when θ_{AsOH} becomes small (eq 6). Second, interactions between As−OH groups and water or neighboring adsorbed species are likely to be different when As−OH coverage is complete or when it is partial. The negative sign of the U_{fb} shift due to the replacement of OH− by H− groups is consistent with a higher electronegativity of surface OH-groups compared to H-groups: $As^{+\delta}(OH)^{-\delta}$ is replaced by $As^{-\delta'}(H)^{+\delta'}$. On the assumption that the capacitance of the dipole layer is about 10^{-4} F cm^{-2},[16] an effective charge variation $[\delta + \delta']$ of about 0.2 e per site can be estimated. Adsorbed OH and H groups have a similar influence on the flatband potential of germanium electrodes, discussed extensively by Gerischer, Memming, and others,[64,73] although surface charges may also play a significant role in that system.[74]

The different parts of the GaAs/solution interface over which changes in applied potential are distributed are summarized in Figure 11, inspired from a similar figure by Gerischer et al.[65] for germanium electrodes. The layer with surface dipoles results in a potential drop $\Delta\phi_{dip}$ due to the orientation of the permanent dipoles $As^{+\delta}(OH)^{-\delta}$, thereby affecting the barrier for electron transfer from GaAs. On the other hand, the negative charge on dissociated OH groups, compensated by a positive charge in solution, largely determines the potential drop $\Delta\phi_H$ across the Helmholtz layer.

4.3. Inventory of Reaction Steps. Adsorption and desorption compete continuously at every surface site. For an understanding of hydrogen adsorption at the electrochemical interface, it is therefore crucial to examine the reaction pathway.

The switch from As−OH to As−H or back requires two charge carriers, implying the presence of a short-lived As$^\bullet$ radical intermediate. Cathodic hydrogenation requires two electrons,

$$As{-}OH + e^- + H^+_{(aq)} \xrightarrow{k_1} As^\bullet + H_2O \quad (7)$$

$$As^\bullet + e^- + H^+_{(aq)} \xrightarrow{k_2} As{-}H \quad (8)$$

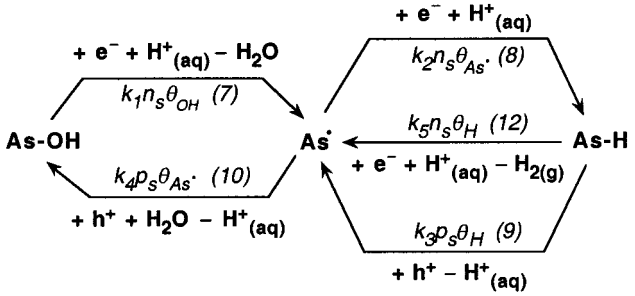

Figure 12. Reaction scheme for changes in surface coverage of GaAs cathodes. Expressions for the rates of the reaction steps are given in italics, as well as numbers referring to the corresponding equations in the text.

while anodic hydroxylation requires two holes

$$As{-}H + h^+ \xrightarrow{k_3} As^\bullet + H^+_{(aq)} \quad (9)$$

$$As^\bullet + h^+ + H_2O \xrightarrow{k_4} As{-}OH + H^+_{(aq)} \quad (10)$$

The factors k_i are positive reaction rate constants. That the oxidation of As−H or As$^\bullet$ does not occur by electron injection into the conduction band is supported by two observations: no electron injection was measured when a (partially) hydrogen-covered cathode was polarized in the anodic range in the dark (Figure 7), and the highest anodic current measured during the coulometric titrations with photogenerated holes was equal to that in the photocurrent plateau, for which electron injection is known to be completely negligible[26] (compare Figures 3a and 6a). It will be assumed that the hole capture steps are irreversible too.

The reduction of a solvated proton, yielding an adsorbed hydrogen atom H_{ads}, is the first step in the mechanism of hydrogen gas evolution at a cathode. Gerischer et al.[12] determined that the formation of a hydrogen molecule requires two conduction-band electrons on GaAs. For a given electrode material and given experimental conditions, an important question is whether the second step proceeds by surface diffusion to another adsorbed hydrogen atom (11a) or by a second charge-transfer step at the same site (11b):[16]

$$H_{ads} + H_{ads} \rightarrow H_{2(g)} \quad (11a)$$

$$H_{ads} + H^+_{(aq)} + e^- \rightarrow H_{2(g)} \quad (11b)$$

For example, the hydrogen evolution route includes reaction step 11a on platinum electrodes and reaction step 11b on gold electrodes.[16] For n-GaAs, the stability of adsorbed hydrogen in the dark in the anodic range (Figures 2 and 7) is direct evidence against there being mobile adsorbed hydrogen atoms which combine to form hydrogen molecules. Therefore, hydrogen evolution proceeds via reaction 11b. The mobility of adsorbed hydrogen is negligible, in line with the covalent character of the As−H bond. Therefore, in the cathodic range, a hydrogen molecule is produced by two consecutive electron-transfer steps at the same site, i.e., reaction step 8 followed by

$$As{-}H + e^- + H^+_{(aq)} \xrightarrow{k_5} As^\bullet + H_{2(g)} \quad (12)$$

An overview of the reaction steps is given in Figure 12. The same scheme is valid at pH 0 and pH 14, as will be discussed in the next section.

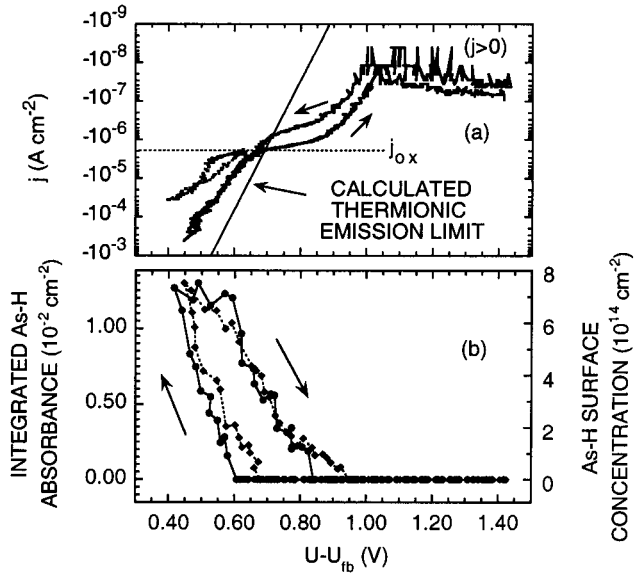

Figure 13. (a) Current density and (b) hydrogen surface coverage plotted against the semiconductor bandbending at pH 0 (same data as Figure 8).

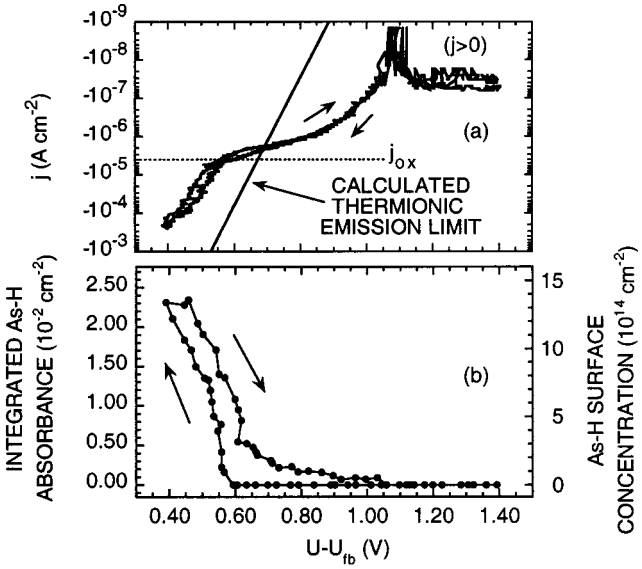

Figure 14. Same as Figure 13, but at pH 14.

4.4. Identification of the Rate-Limiting Step. Cathodic hydrogen gas evolution on GaAs occurs according to reactions 8 and 12. Considering the expected high reactivity of surface radical As$^{\bullet}$ species, coverage by As$^{\bullet}$ is probably very small. This conclusion is supported by two arguments on the basis of our experimental results. First, the direct correlation of U_{fb} with θ_H (Figure 10) suggests that the surface composition has only one degree of freedom. Since replacing AsH by As$^{\bullet}$ or AsOH should have two significantly different effects on the surface dipole potential, one concludes that adsorbed H is always replaced by the same species, adsorbed OH. As a result, most surface sites must be either OH- or H-terminated, and coverage by As$^{\bullet}$ is very low. A second argument is the observed high coverage by hydrogen at the most negative potentials. It is concluded that $k_5 \ll k_2$, meaning that the hydrogenation of As−H is rate limiting for hydrogen evolution (see Figure 12). This conclusion is consistent with the mechanistic view of a simplified two step mechanism: As → As−H → As + H_2. Near unity surface coverage by As−H stands as a clear-cut proof that the second step is rate limiting.

The hydrogenation of adsorbed hydrogen involves the transfer of an electron and that of a proton. All experimental evidences indicate that the two transfers are not simultaneous. Electron transfer depends on the concentration n_s of electrons at the surface and thus on $(U - U_{fb}) = \Delta\phi_{sc}$:[30]

$$n_s = N_D e^{-e(U-U_{fb})/k_B T} \tag{13}$$

In contrast, ion transfer depends on the potential drop on the solution side of the interface, affected by variations of U_{fb} directly ($= \Delta\phi_{dip} + \Delta\phi_H$), not $(U - U_{fb})$. Figures 13 and 14 replot the data of Figure 8 as j and θ_H versus $(U - U_{fb})$. Comparison shows that when the surface electron concentration is the same, the current density is practically the same at pH 0 and at pH 14. Moreover, in both figures, j shows much less hysteresis than in the $j-U$ curves in Figure 8a. This indicates that current density depends essentially on the electron concentration at the surface. If proton transfer over the Helmholtz layer had been rate limiting, then, under conditions of constant pH (fulfilled in Figures 8, 13, and 14), current density during the forward and the reverse scan would not have been the same for a same value of n_s, but rather for a same value of θ_H.

Since it was already concluded that the hydrogenation of As−H is rate limiting, it can now be concluded that the rate-limiting step is electron transfer to As−H sites. This seems very plausible, since electron transfer is expected to be much faster to very reactive As$^{\bullet}$ surface radical sites than to much more stable As−H sites, and the electric field in the Helmholtz layer is very favorable for the arrival of protons to neutralize transferred negative charge (Figure 11). An interesting parallel can be drawn with the anodic dissolution of semiconductors: proposed mechanisms also often involve reaction steps in which rate determining charge transfer is alternated with rapid chemical neutralization of the transferred charge.[26,75]

Most authors make the distinction between $H^+_{(aq)}$ reduction at pH 0 and H_2O reduction at pH 14.[12,16] This is because the overall reaction is

$$2H^+_{(aq)} + 2e^- \rightarrow H_2\uparrow \tag{14}$$

in acidic solutions and

$$2H_2O + 2e^- \rightarrow H_2\uparrow + 2OH^-_{(aq)} \tag{15}$$

in alkaline solutions. However, since electron transfer is rate-limiting here, the source of protons is of no importance for the reaction rate. It makes no difference to assume that $H^+_{(aq)}$ is reduced over the entire pH range and that at pH 14, $H^+_{(aq)}$ originates from the water dissociation equilibrium,

$$H_2O \rightleftarrows H^+_{(aq)} + OH^-_{(aq)} \tag{16}$$

It is often assumed that rates of electrochemical charge-transfer steps are proportional to the surface concentrations of reduced or oxidized surface sites and to the surface concentration of the electrons or holes. On this basis, taking reaction 12 as rate limiting, the total current density could be expressed as $-2k_5N_s\theta_H n_s e$, where N_s is the total density of surface sites. If this were true, the hysteresis in j vs $(U - U_{fb})$ between forward and reverse scans (Figures 13a and 14a) would be much larger, because θ_H vs $(U - U_{fb})$ shows significant hysteresis. The very small hysteresis indicates that the majority of the current is due to charge transfer at a minority of the As−H sites. This is in agreement with the observation that, at a same potential, current density increases considerably during the first current−potential cycles while θ_H and U_{fb} remain approximately unchanged. For

a same surface electron concentration, surface roughening increases current density by increasing the number of active sites through which most of the current passes.

In most of the present study, metallic surface gallium resulting from cathodic decomposition of GaAs was avoided by maintaining the applied potential outside the thermodynamic stability range of metallic gallium. For metallized semiconductor electrodes, current densities are often limited by thermionic emission, i.e., all electrons which reach the semiconductor surface are transferred.[30,39,76] The current density is then given by:

$$j \approx A^* T^2 \exp(-e\Delta\phi_{sc}/k_B T) \qquad (17)$$

where A^* is ≈ 8 A cm^{-2} K^{-2} for GaAs.[30,77] In Figures 13 and 14, no metallic gallium is present, and current density during hydrogen gas evolution is lower than the thermionic emission limit, but not to a very large extent. The much lower current density obtained for a polished electrode not yet cathodically pretreated supports the conclusion that a majority of the current flows through a minority of very reactive surface sites at the microrough surface.

At potentials where oxygen is reduced at a rate below the oxygen diffusion limit, the negative current density significantly exceeds the calculated thermionic emission limit. This is surprising, since in the thermionic emission limit, all electrons which reach the surface are transferred and a higher current density would seem impossible. Due to its negative sign, the current must nevertheless be an electron current. It could at first be surmised that holes are injected and that they recombine with electrons within the semiconductor at a short distance from the surface, where the electron density in the conduction band is much higher. However, measurements on p-GaAs electrodes under reverse bias indicate the absence of hole injection ($|j| < 0.05$ μA cm^{-2}) under conditions where diffusion-limited O_2 reduction attains -100 μA cm^{-2} on n-type GaAs. An alternative explanation is that the barrier height for electron transfer is not homogeneous over the entire surface. Since the electron transfer rate increases exponentially with decreasing barrier height, a majority of the current could pass through a minority of the sites, while the measured $e(U - U_{fb})$ represents an average barrier height determined essentially by the majority of the sites. The flatband potential of GaAs electrodes is known to depend on the exposed crystallographic face,[24,25] so that the barrier height could be different for morphologically different sites at the microrough surface. Moreover, either one or two OH- or H-groups can be attached to a surface arsenic atom, depending on the site, which should have a marked influence on the local barrier height. It should however be kept in mind that charge-transfer rates depend not only on the barrier height inside the semiconductor, but also on the energy overlap between the semiconductor bands and the surface species.

On the basis of our experimental results, two comments can be made regarding theories which other authors have assumed to be valid for hydrogen gas evolution on GaAs. First, it should now be clear that it is incorrect to assume that the charge-transfer steps are activated across the Helmholtz layer,[23,24] because the electrons are transferred to surface sites, without passing through the Helmholtz layer. Second, hydrogen gas evolution on GaAs cathodes is not suitable to test the validity of theories putting an upper limit on rates of direct charge transfer to dissolved electrolyte species, in contrast to the suggestion by Nozik and Memming:[78] even when the cathodic hydrogen gas evolution rate is limited by thermionic emission, hydrogen evolution is bound to be a two-step process with an adsorbed hydrogen intermediate. And it should not be forgotten that even for reversible one-electron redox systems, mediation by surface species can greatly enhance rates of electron transfer at semiconductor electrodes, as was argued by Vanmaekelbergh.[79,80]

4.5. Dynamic Potential Dependence of θ_H and j. It is now possible to examine whether the dynamic potential dependence of hydrogen surface coverage and current density can be explained on the basis of the microscopic mechanism described above. The origin of the hystereses in θ_H and j during cyclic potential scans and the approximately linear dependence of θ_H on the applied potential are of special interest.

It was found that the hydrogen gas evolution current density is directly proportional to the concentration n_s of free electrons at the surface. Furthermore, at constant pH and given potential, changes in n_s are essentially due to changes in hydrogen surface coverage, through $\Delta\phi_{dip}$ and U_{fb} (see eqs 2, 3, and 13). Hysteresis in j during cyclic potential scans is thus directly due to hysteresis in θ_H. An explanation of the hysteresis in θ_H therefore simultaneously accounts for the hysteresis in j.

θ_H results from a balance between reaction steps which adsorb and steps which desorb hydrogen. It is often assumed that hydrogen surface coverages of cathodes are determined by the relative rate constants of the two steps of the hydrogen gas evolution reaction.[16] However, with GaAs, the θ_H dependence on potential is clearly not merely due to a balance between steps 8 and 12, since the ratio of the rate constants of those steps (k_2/k_5) does not depend on potential—no activation occurs across the Helmholtz layer during rate-limiting electron transfer to As$^\bullet$ and AsH surface sites. Steps creating or removing adsorbed OH-groups are crucial in determining θ_H, and a general origin for hysteresis is the fact that an increase in θ_H requires different reactants than a decrease in θ_H: an increase in θ_H requires electrons from the conduction band, whereas a decrease in θ_H requires oxidants to convert As$^\bullet$ into AsOH, else As$^\bullet$ is immediately rehydrogenated (Figure 12).

The hydrogenation mechanism was addressed in detail in the previous sections. The inverse process, hydroxylation, requires holes or, in the absence of an anodic current, it can occur by chemical reaction with oxygen (Figure 2). The current density corresponding to the flow of oxygen toward the surface will be referred to as j_{ox} and the current density of electrons transferred from the conduction band as j_e. When $|j_e| > |j_{ox}|$, all oxygen which reaches the surface is reduced cathodically. Nevertheless, since cathodic oxygen reduction at GaAs occurs partially via the valence band,[81] a hole current density of the order of j_{ox} is injected under cathodic conditions, which may contribute to the oxidation of surface species.

During negative potential scans, hydrogen gas evolution begins at a somewhat more negative potential than the H_2/H^+ redox potential [$E°(H_2/H^+) = -0.20$ V vs Ag/AgCl(saturated KCl)]: AsH appears when $|j_e| > |j_{ox}|$. θ_H increases more or less linearly with U during the negative scan, in such a way that a large part of changes in applied potential falls across the Helmholtz layer. When the scan direction is reversed, θ_H does not start to decrease immediately. In fact, closer inspection of Figure 8 reveals that θ_H does not start to decrease before current density has dropped back to about j_{ox}, i.e., when the electron flow is no longer sufficient to reduce all the oxidant molecules which reach the surface from solution. This is even clearer in Figure 15, in which θ_H is plotted against j. With deaerated solutions, the transition current density j_{ox} is of the order of 1 μA cm^{-2} (Figure 15a,b), while with oxygen-saturated solutions, it is of the order of 100 μA cm^{-2} (Figure 15c). The apparent condition that θ_H will not decrease before $|j_e| < |j_{ox}|$ describes

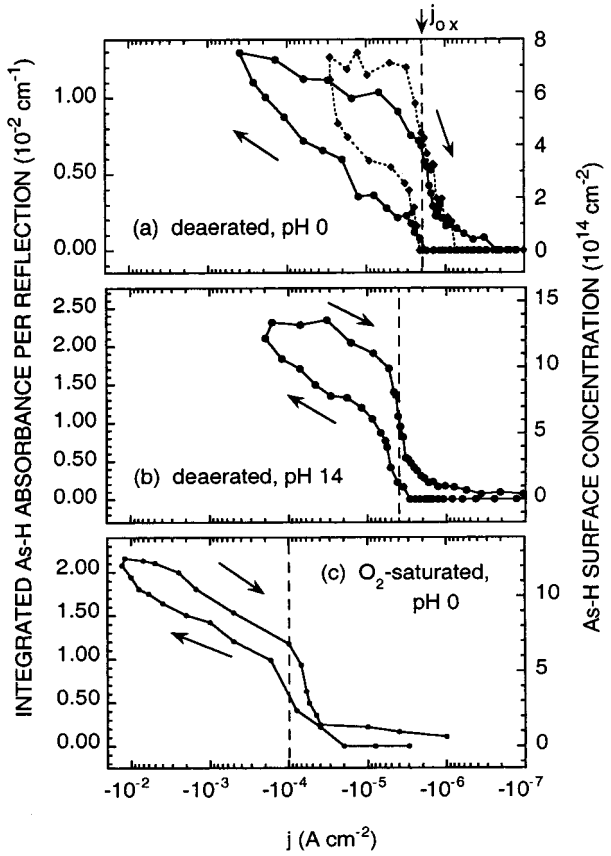

Figure 15. Hydrogen surface coverage of n-GaAs electrodes as a function of the current density on a logarithmic scale for deaerated solutions of (a) 1 M HCl and (b) 1M NaOH (same data as Figure 8) and (c) for an oxygen-saturated solution of 1 M HCl.

the hysteresis at low potential scan rates, for which it was already remarked elsewhere[11] that hysteresis becomes essentially independent of the potential scan rate. At high potential scan rates (Figure 6), the additional hysteresis occurs because the highest rate at which adsorbed hydrogen can be removed is equal to j_{ox}. Although Figures 13b and 14b evoke a Frumkin isotherm for adsorbed species showing strong attractive interaction,[82,83] the pivotal role of j_{ox} (Figure 15) clearly demonstrates that the origin of the present hystereses is kinetic, not thermodynamic. An explanation must therefore be sought in the reaction mechanism.

The magnitudes of the rate constants in the reaction scheme in Figure 12 are now examined. It was already concluded that $k_2 \gg k_5$ —AsH hydrogenation is the rate-limiting step in hydrogen gas evolution. Since θ_H and θ_{OH} are more or less of the same order of magnitude while hydrogen evolution is the dominant reaction, it can also be concluded that $k_5 \gg k_1$. The hole current is distributed over the oxidation of AsH and that of As•. The rapid scan in the positive direction in Figure 6 indicates that when an AsH surface is oxidized to AsOH, the surface does not go through an intermediate situation where it is mainly covered with As•, because AsH and U_{fb} would be less well correlated. Hence, when an AsH site is oxidized anodically to As•, it is immediately further oxidized to AsOH, so that $k_4 \gg k_3$ in the reaction scheme. The conclusions that $k_2 \gg k_5$ and $k_4 \gg k_3$ agree with the expectation that a surface radical like As• is much more reactive than AsOH and AsH sites. The high reactivity of As• could be part of the explanation for the high surface recombination rates of photogenerated electron−hole pairs at GaAs electrodes[32] (see the $j \approx 0$ plateau in Figure 6). For germanium, Memming and Neumann also postulated that the radical intermediate in the hydrogen evolution reaction is a very efficient recombination center.[84,85]

Despite the conclusion that $k_4 \gg k_3$, a majority of holes might nevertheless be consumed in the oxidation of AsH instead of As• during cathodic hydrogen gas evolution. The reason is that the reaction rates depend not only on the rate constants but also on the surface coverages. If $(k_2/k_5) \gg (k_4/k_3)$, both $(k_4 \gg k_3)$ and $k_3\theta_H \gg k_4\theta_{As\bullet}$ can be valid simultaneously, because $(\theta_H/\theta_{As\bullet}) \approx (k_2/k_5)$ when hydrogen gas evolution is the dominating reaction. In this way, only a minute fraction of the holes is available for the oxidation of As• to AsOH during reverse scans, so that, except at extremely low scan rates, θ_H does not decrease during reverse scans before $|j_e| < |j_{ox}|$.

In the steady state, the oxidation of As• to AsOH must be balanced by the reduction of AsOH sites. On the assumption that the current density due to the latter process is given by $-ek_1N_s\theta_{OH}n_s$, one of the steady-state conditions is

$$\frac{k_4\theta_{As\bullet}}{k_3\theta_H} j_{ox} = ek_1N_s\theta_{OH}n_s \qquad (18)$$

The dependence of U_{fb} on θ_H is approximated by a linear relation (Figure 10):

$$U_{fb}(\theta_H) = U_{fb}(\theta_H = 0) + \beta\,\theta_H \qquad (19)$$

where $\beta < 0$. With eq 13 and $(\theta_H/\theta_{As\bullet}) \approx (k_2/k_5)$, the last two equations lead to the following expression for θ_H:

$$\theta_H \approx \frac{1}{\beta} U - \frac{1}{\beta} U_{fb}(\theta_H = 0) - \frac{k_BT}{\beta e} \ln \frac{ek_1N_sN_D(1-\theta_H)}{(k_4k_5/k_2k_3)j_{ox}} \qquad (20)$$

The general origin of the linear potential dependence of θ_H during negative scans is clear: a large part of changes in applied potential falls across the surface dipole layer, while U_{fb} shifts more or less linearly with θ_H (eq 19).

The dynamic potential dependence of hydrogen surface coverage under illumination or in the dark was simulated numerically on the basis of the reaction scheme in Figure 12. The method is detailed in the Appendix. Resulting $j-U$ and θ_H-U curves are presented in Figures 16 and 17. The simulated behavior is in general agreement with the experiments (compare with Figures 6 and 8, respectively). Under illumination ($j_{ox} = j_{photo}$), a photocurrent equal to j_{ox} flows anodically, and it is compensated by the electron current j_e at the open circuit potential. In the dark ($j_{ox} = j_{O_2}$), j_e compensates j_{ox} when all oxygen which arrives at the surface is reduced cathodically. In terms of j_e and j_{ox}, the behaviors under illumination and in the dark are very much alike. Hysteresis of the current−potential curves is the largest during rapid scans, and some hysteresis remains even during very slow scans. Simulated coverage by As• is negligible with respect to θ_H and θ_{OH}, so that $\theta_{OH} \approx 1 - \theta_H$. When $|j_e|$ equals $|j_{ox}|$, electrons convert AsOH into As• and holes As• back into AsOH, i.e., As• acts as a recombination center. At more negative potentials, $|j_e|$ exceeds $|j_{ox}|$, and excess electrons lead to AsH and its hydrogenation: hydrogen gas is evolved. During a slow scan, θ_H begins to increase sooner than in a rapid scan, leading to a larger negative shift in flatband potential and hence to a lower current density. θ_H increases as potential becomes more negative, but it remains lower than the value which would cause the entire change in applied potential to drop across the surface dipole layer; otherwise, band bending would no longer change and there would no longer be a driving force for θ_H to change either. The Tafel slope during scans in the negative direction is very much dependent on the value for

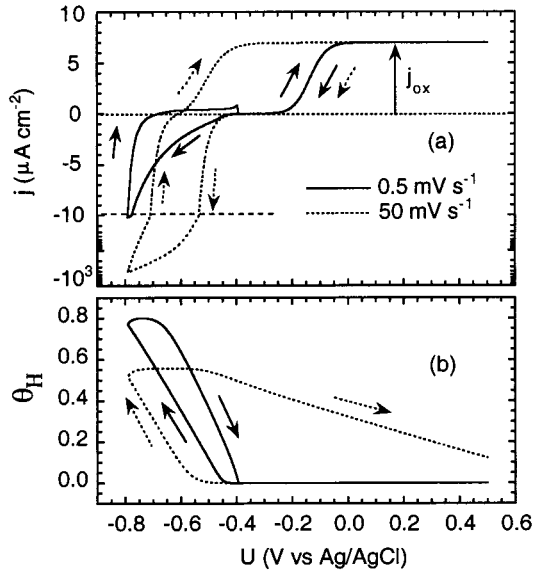

Figure 16. Numerical simulations of the dynamic potential dependence of (a) current density and (b) hydrogen surface coverage according to the reaction scheme in Figure 12. Notice the similarity with Figure 6a,b. The photohole current density is given by $j_{ox} = 7 \times 10^{-6}$ A cm^{-2}, and the following values were chosen for the rate constants: $k_1 = 10^{-13}$ cm^3 s^{-1}, $k_2 = 10^{-7}$ cm^3 s^{-1}, $k_3 = 10^{-12}$ cm^3 s^{-1}, $k_4 = 10^{-11}$ cm^3 s^{-1}, $k_5 = 10^{-12}$ cm^3 s^{-1}, $k_6 = 10^{-14}$ cm^3 s^{-1}, $k_7 = 10^{-2}$ cm^3 s^{-1}, and $k_8 = 10^{-10}$ cm^3 s^{-1}. Other input parameters were $U_{fb}(\theta_H = 0) = -0.85$ V vs Ag/AgCl, $\beta = -0.4$ V per monolayer (eq 19), $N_s = 10^{15}$ cm^{-2}, $T = 300$ K, and $N_D = 7 \times 10^{16}$ cm^{-3}.

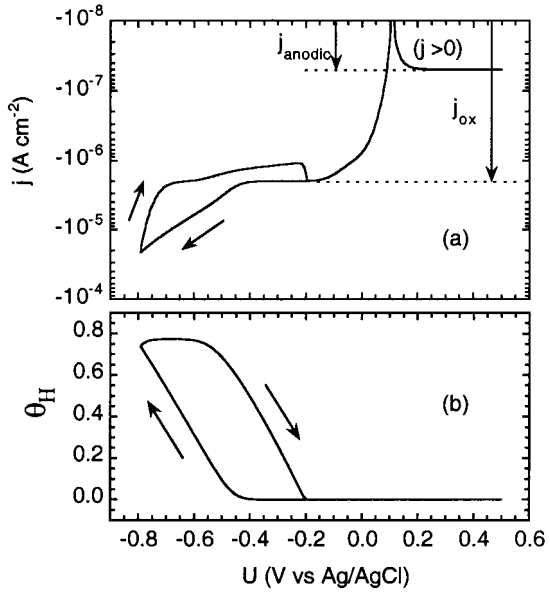

Figure 17. Same as Figure 16, but in the dark—$j_{ox} = 2 \times 10^{-6}$ A cm^{-2} now represents the rate at which oxygen arrives at the surface, and $j_{anodic} = 5 \times 10^{-8}$ A cm^{-2} is the reverse bias current thermally generated inside the semiconductor depletion layer (scan rate = 1 mV s^{-1}). Notice the similarity with measurements at pH 0 shown in Figure 8a,b. For k_9 and k_{ch} (eq 25), it is assumed that $k_9 = (10^{-2}$ cm$^3) \times k_{ch}$.

β in eq 19 but is also affected in a complex way by the rate constants. During reverse scans, θ_H at first remains constant, because most holes are consumed in the oxidation of AsH to As$^\bullet$, which is rapidly rehydrogenated. Since changes in applied potential fall almost exclusively across the semiconductor space charge layer, the Tafel slope is (k_BT/e) ln(10). Only when the flow of oxidants toward the surface is no longer compensated by the flow of electrons does AsH decrease. The highest rate at which AsH can disappear corresponds to j_{ox}.

The simulation in Figure 17 reveals an effect which one could easily have overlooked in Figure 8: between the potential where AsH first appears during the negative scan and the potential where AsH is no longer present during the positive scan, current density is higher during the forward scan compared to the reverse scan by a factor of 2. This is related to the fact that cathodic oxygen reduction on GaAs occurs for one-half via the conduction band and for one-half via the valence band. Two electrons are transferred to each oxygen molecule, leading to the injection of two holes. During the scans in negative direction, the electron concentration at the surface is sufficiently high that the injected holes recombine with electrons, so that four electrons are measured per oxygen molecule. During the scans in positive direction, the electron concentration at the surface is much lower at the same potentials, due to the presence of surface hydrogen and its effect on semiconductor bandbending, so that the injected holes do not recombine with electrons but lead to the dissolution of GaAs: only two electrons are measured per oxygen molecule.

Differences between the simulations and the experiments are in part due to experimental complications not taken into account in the simulations. Irreversible surface changes were not taken into account, nor was the role of a minority of extremely reactive sites. The potential- and time-dependent coverage by positively charged anodic dissolution intermediates could have been included in Figure 16, leading to shifts of the flatband potential and to a less abrupt change from zero current to the photocurrent plateau. Chemical oxidation by oxygen was neglected in Figure 16, and its kinetics were oversimplified in Figure 17—depending on the kinetics, time-dependent changes of the local oxygen concentration could affect the curves too. Despite all such simplifications, the simulations reproduce most essential features of the experiments. It can be concluded that the hysteresis and other dynamic behavior observed cathodically under illumination and in the dark can be quite well understood on the basis of the simple reaction scheme in Figure 12.

5. Conclusion

The microscopic mechanism of hydrogen gas evolution on GaAs cathodes has been unraveled by in situ infrared spectroscopy. Surface hydrogen is bound to arsenic atoms and replaces surface OH-groups present under anodic conditions, causing a change in the surface dipole potential. Electron transfer to As−H sites is rate-determining for the hydrogen gas evolution reaction, so that the microscopic reaction mechanism is pH-independent. During potential scans in a negative direction, hydrogen surface coverage increases linearly with potential in such a way that changes in applied potential fall in large part across the dipole layer. During positive scans, θ_H remains constant until the current density due to the transfer of electrons from the conduction band no longer exceeds the flow of oxidants toward the surface. Since a change in θ_H affects the surface electron concentration at constant potential, the hysteresis in θ_H during potential cycles is the cause of the hysteresis in the current density.

The techniques applied here can also be applied to investigate the electrochemical behavior of other materials. A recent example is the in situ infrared spectroscopic study of germanium electrodes which reveals how the dynamic current−potential behavior is correlated to variations in the surface concentrations of adsorbed hydroxyl groups, adsorbed hydrogen atoms, and free charge carriers.[74] The fundamental knowledge acquired on n-GaAs electrodes in indifferent electrolyte solutions forms a basis for investigations of more complex systems, such as GaAs

electrodes in the presence of hydrogen peroxide. The latter chemical is commonly used in GaAs surface preparation technology,[25,26,86,87] although its electrochemical behavior is not yet completely understood—the current density exhibits stable periodic oscillations in the cathodic range.[88,89] It will be shown in another paper that such effects are strongly correlated to variations in surface chemistry.[90]

Acknowledgment. The authors thank D. Vanmaekelbergh, J. J. Kelly, D. Paget, and F. Maroun for helpful discussions, F. Maroun for help with the numerical fitting of infrared spectra, J. J. Kelly for GaAs material, and the European Commission for a TMR Research Training Grant (B.H.E.).

APPENDIX Numerical Simulation of the Current-Potential Curves

Details are given of the method by which current−potential curves were simulated numerically (Figures 16 and 17).

Despite comments concerning the role of a minority of extremely reactive sites, the rate of each reaction step is taken to be proportional to the surface coverage of the species reduced or oxidized and to the concentration n_s of free electrons or p_s of free holes, respectively. The contributions of the steps to the current density are thus assumed to be $-ek_1N_s\theta_{OH}n_s$, $-ek_2N_s\theta_{As\bullet}n_s$, $+ ek_3N_s\theta_H p_s$, $+ek_4N_s\theta_{As\bullet}p_s$, and $-ek_5N_s\theta_H n_s$. N_s is set at 10^{15} cm^{-2}. It is assumed that oxidations are due to a flow of oxidants corresponding to a current density j_{ox}. The flatband potential $U_{fb}(\theta_H = 0)$ in the anodic range is taken to be −0.85 V vs Ag/AgCl, linear U_{fb} dependence on θ_H is assumed ($\beta = -0.4$ V per monolayer, eq 19), and charge by surface intermediates is neglected.

Under illumination, j_{ox} represents the photohole current density j_{photo}. Under stationary conditions in the anodic range, $j_{ox} = 2ek_6N_s\theta_{OH}p_s$ is taken to lead to dissolution of the semiconductor:

$$\mathrm{AsOH} + \mathrm{h}^+ \xrightarrow{k_6 p_s} \mathrm{ox.} \tag{21}$$

$$\mathrm{ox.} + \mathrm{e}^- \xrightarrow{k_7 n_s} \mathrm{AsOH} \tag{22}$$

$$\mathrm{ox.} + \mathrm{h}^+ \xrightarrow{k_8 p_s} \mathrm{AsOH} + \text{dissolution products} \tag{23}$$

Equation 22 is included in order to simulate surface recombination of photogenerated holes with electrons at photoanodic dissolution intermediates. A value of 10^{-14} cm^3 s^{-1} is taken for k_6, corresponding to the value found by Lingier et al.[91] for p-GaAs anodes in aqueous solutions; k_3 and k_4 were chosen according to $k_6 \ll k_3 \ll k_4$ [$k_6 \ll k_3$, because all anodic current goes toward the oxidation of surface hydrogen as long as AsH is present (Figures 4 and 6)]. k_7 and k_8 were chosen according to $k_7\theta_{ox} \gg k_1\theta_{OH}$ and $k_8 \gg k_6$, so that coverage by "ox." always remains very small and the surface is essentially OH-covered in the anodic range. Surface coverage θ_{ox} by dissolution intermediate "ox." is assumed to be in a steady state:

$$\theta_{ox} = \frac{k_6 p_s}{k_7 n_s + k_8 p_s}\,\theta_{OH} \tag{24}$$

In the dark, $j_{ox} = j_{O_2}$ is taken to correspond to a potential-independent rate at which oxygen arrives at the surface. Part of the oxygen is reduced cathodically, for one half by taking electrons from the conduction band and for one half by injecting holes into the valence band ("current doubling"[81]). The remaining oxygen is assumed to oxidize AsH and As$^\bullet$ chemically (for simplicity, one and the same rate constant k_{ch} is taken for AsH and As$^\bullet$). The electron transfer rate to dissolved oxygen is taken proportional to $-ek_9n_s$ under conditions where it is kinetically limited, resulting in an electron transfer current density and a hole current density of equal magnitude j_h:

$$j_h = \left(\frac{j_{O_2}}{2}\right)\frac{k_9 n_s}{k_9 n_s + k_{ch}} \tag{25}$$

In addition to j_h in the dark and the photogeneration current density j_{photo} under illumination, another source of holes at the surface is the small reverse bias current density j_{anodic} thermally generated in the semiconductor space charge layer, fixed at 50 nA cm^{-2} in the simulations (in principle, it is proportional to the square root of band bending[30]). The concentration p_s of holes at the surface is assumed to approximate a steady state:

$$p_s = \frac{j_{photo} + j_{anodic} + j_h}{(k_3\theta_H + k_4\theta_{As\bullet} + k_6\theta_{OH} + k_8\theta_{ox})N_s e} \tag{26}$$

The concentration n_s of electrons at the surface is calculated using eq 13, on the assumption that only a fraction of the electrons reaching the surface are transferred. The electron capture constants are chosen according to $k_1 \ll k_5 \ll k_2$ and $(k_2/k_5) \gg (k_4/k_3)$.

Starting in the anodic range with $\theta_{OH} = 1$, $\theta_{As\bullet} = 0$, and $\theta_H = 0$, the applied potential is slowly changed at a chosen scan rate in increments corresponding to time steps of 1 μs. After each U increment, the resulting new values of p_s and n_s are calculated (eqs 26 and 13) and from that the changes in θ_H, $\theta_{As\bullet}$, and θ_{OH}:

$$\Delta\theta_{As\bullet} = \left(k_1\theta_{OH}n_s + k_3\theta_H p_s + k_5\theta_H n_s - k_2\theta_{As\bullet}n_s - k_4\theta_{As\bullet}p_s - (j_{O_2} - 2j_h)\frac{\theta_{As\bullet}}{\theta_{As\bullet} + \theta_H}\right)\Delta t \tag{27}$$

$$\Delta\theta_H = \left(k_2\theta_{As\bullet}n_s - k_5\theta_H n_s - k_3\theta_H p_s - (j_{O_2} - 2j_h)\frac{\theta_H}{\theta_{As\bullet} + \theta_H}\right)\Delta t \tag{28}$$

$$\Delta\theta_{OH} = -\Delta\theta_{As\bullet} - \Delta\theta_H \tag{29}$$

From the new value of θ_H, the new value of U_{fb} is calculated (eq 19). Finally, the total (electron) current density is determined:

$$j = j_{photo} + j_{anodic} - j_h - eN_s(k_1\theta_{OH}n_s + k_2\theta_{As\bullet}n_s + k_5\theta_H n_s + k_7\theta_{ox}n_s) \tag{30}$$

The j_{photo} and j_{anodic} terms are included because they correspond to the generation of electron−hole pairs. The electrons move toward the inside of the semiconductor, due to the electric field, and are measured in the external circuit if the holes do not recombine with electrons at the surface. The j_h term has a negative sign, because it corresponds to the transfer of electrons from the semiconductor to dissolved oxygen. The last four terms are negative also, since they correspond to the transfer of electrons from the semiconductor to surface sites.

List of Frequently Used Symbols

U	applied potential (V vs Ag/AgCl)
U_{fb}	flatband potential (V vs Ag/AgCl)
U_{stat}	stationary potential during transient capacitance measurements (V vs Ag/AgCl)
j	total current density (A cm^{-2})
j_{ox}	current density corresponding to the flow of oxidants toward the surface (A cm^{-2})
j_e	current density of electrons transferred from the conduction band (A cm^{-2})
e	the positive elementary charge (C)
k_B	the Boltzmann constant (eV K^{-1})
T	absolute temperature (K)
θ_H, θ_{OH}, ...	fractional surface coverage by H, OH, ...
N_s	total concentration of surface sites (cm^{-2})
k_i	positive reaction rate constant of step i (cm^3 s^{-1})
N_D	dopant density (cm^{-3})
n_s	concentration of free electrons at the surface (cm^{-3})
p_s	concentration of free holes at the surface (cm^{-3})

References and Notes

(1) Pearton, S. J.; Corbett, J. W.; Shi, T. S. *Appl. Phys. A* **1987**, *43*, 153.

(2) Chevallier, J.; Aucouturier, M. *Annu. Rev. Mater. Sci.* **1988**, *18*, 219.

(3) Chevallier, J.; Clerjaud, B.; Pajot, B. In *Hydrogen In Semiconductors, Semiconductors and Semimetals*; Pankove, J. I., Johnson, N. M., Eds.; Academic: New York, 1990; Vol. 34, Chapter 13.

(4) Rahbi, R.; Pajot, B.; Chevallier, J.; Marbeuf, A.; Logan, R. C.; Gavand, M. *J. Appl. Phys.* **1993**, *73*, 1723.

(5) Yablonovitch, E.; Allara, D. L.; Chang, C. C.; Gmitter, T.; Bright, T. B. *Phys. Rev. Lett.* **1986**, *57*, 249.

(6) Nichols, R. J.; Bewick, A. *J. Electroanal. Chem.* **1988**, *243*, 445.

(7) Ogasawara, H.; Ito, M. *Chem. Phys. Lett.* **1994**, *221*, 213.

(8) Peremans, A.; Tadjeddine, A. *Phys. Rev. Lett.* **1994**, *73*, 3010.

(9) Peremans, A.; Tadjeddine, A. *J. Electroanal. Chem.* **1996**, *409*, 115.

(10) Ren, B.; Huang, Q. J.; Cai, W. B.; Mao, B. W.; Liu, F. M.; Tian, Z. Q. *J. Electroanal. Chem.* **1996**, *415*, 175.

(11) Erné, B. H.; Stchakovsky, M.; Ozanam, F.; Chazalviel, J.-N. *J. Electrochem. Soc.* **1998**, *145*, 447.

(12) Gerischer, H.; Müller, N.; Haas, O. *J. Electroanal. Chem.* **1981**, *119*, 41.

(13) Gerischer, H.; Mattes, I. *Z. Phys. Chem. Neue Folge* **1966**, *49*, 112.

(14) Uosaki, K.; Kita, H. *J. Am. Chem. Soc.* **1986**, *108*, 4294.

(15) Erné, B. H.; Ozanam, F.; Chazalviel, J.-N. *Phys. Rev. Lett.* **1998**, *80*, 4337.

(16) Bockris, J. O'M.; Reddy, A. K. N. *Modern Electrochemistry*; Plenum: New York, 1970; Vol. 2.

(17) Aspnes, D. E.; Studna, A. A. *Phys. Rev. B* **1983**, *27*, 985.

(18) da Fonseca, C.; Ozanam, F.; Chazalviel, J.-N. *Surf. Sci.* **1996**, *365*, 1.

(19) Chazalviel, J.-N. *Electrochim. Acta* **1992**, *37*, 865.

(20) Gee, P. E.; Hicks, R. F. *J. Vac. Sci. Technol. A* **1992**, *10*, 892.

(21) Qi, H.; Gee, P. E.; Hicks, R. F. *Phys. Rev. Lett.* **1994**, *72*, 250.

(22) Venkateswara Rao, A.; Ozanam, F.; Chazalviel, J.-N. *J. Electrochem. Soc.* **1991**, *138*, 153.

(23) Brummer, K. D. N. *J. Electrochem. Soc.* **1967**, *114*, 1274.

(24) Frese, K. W., Jr. *Studies of Physical and Theoretical Chemistry*, Vol. 55: *Semiconductor Electrodes*; Finklea, H. O., Ed.; Elsevier: Amsterdam, 1988.

(25) Notten, P. H. L.; van den Meerakker, J. E. A. M.; Kelly, J. J. *Etching of III−V Semiconductors, An Electrochemical Approach*; Elsevier Advanced Technology: Oxford, 1991.

(26) Gomes, W. P.; Goossens, H. H. In *Advances in Electrochemical Science and Engineering*; Gerischer, H., Tobias, C. W., Eds.; VCH: Weinheim, 1994; Vol. 3.

(27) Rappich, J.; Lewerenz, H. J.; Gerischer, H. *J. Electrochem. Soc.* **1993**, *140*, L187.

(28) Maroun, F.; Ozanam, F.; Chazalviel, J.-N. *Chem. Phys. Lett.* **1998**, *292*, 493.

(29) Higashi, G. S.; Chabal, Y. J.; Trucks, G. W.; Raghavachari, K. *Appl. Phys. Lett.* **1990**, *56*, 656.

(30) Sze, S. M. *Physics of Semiconductor Devices*; Wiley: New York, 1981.

(31) Schröder, K.; Memming, R. *Ber. Bunsen-Ges. Phys. Chem.* **1985**, *89*, 385.

(32) Li, J.; Peter, L. M. *J. Electroanal. Chem.* **1986**, *199*, 1.

(33) Pankove, J. I. *Optical Processes in Semiconductors*; Prentice Hall: Englewood Cliffs, 1971.

(34) Chantre, A.; Vincent, G.; Bois, D. *Phys. Rev. B* **1981**, *23*, 5335.

(35) Hofmann, D. M.; Meyer, B. K.; Lohse, F.; Spaeth, J.-M. *Phys. Rev. Lett.* **1984**, *53*, 1187.

(36) Allongue, P.; Cachet, H.; Horowitz, G. *J. Electrochem. Soc.* **1983**, *130*, 2352.

(37) Vanmaekelbergh, D.; Gomes, W. P.; Cardon, F. *Ber. Bunsen-Ges. Phys. Chem.* **1985**, *89*, 994.

(38) Allongue, P.; Blonkowski, S.; Lincot, D. *J. Electroanal. Chem.* **1991**, *300*, 261.

(39) Uhlendorf, I.; Reineke-Koch, R.; Memming, R. *Ber. Bunsen-Ges. Phys. Chem.* **1995**, *99*, 1082.

(40) Kolthoff, I. M.; Miller, C. S. *J. Am. Chem. Soc.* **1941**, *63*, 1013.

(41) Geffeken, G. *Z. Phys. Chem.* **1904**, *49*, 257.

(42) The Chemical Rubber Co. *Handbook of Chemistry and Physics*, 78th ed.; 1997.

(43) Maroun, F.; Ozanam, F.; Chazalviel, J.-N. *J. Electroanal. Chem.* **1997**, *435*, 225.

(44) Chabal, Y. J. *Surf. Sci. Rep.* **1988**, *8*, 211.

(45) Landolt-Börnstein, *Numerical Data and Functional Relationships in Science and Technology*; Springer-Verlag: Berlin, 1960; Vol. 2−7, p 259.

(46) Koinuma, M.; Uosaki, K. *J. Electroanal. Chem.* **1996**, *409*, 45.

(47) Allongue, P.; Cachet, H. *Electrochim. Acta* **1988**, *33*, 79.

(48) Yamamoto, A.; Yano, S. *J. Electrochem. Soc.* **1975**, *122*, 260.

(49) Tarui, Y.; Komiya, Y.; Harada, Y. *J. Electrochem. Soc.* **1971**, *118*, 118.

(50) Uosaki, K.; Koinuma, M.; Kondo, T.; Ye, S.; Yagi, I.; Noguchi, H.; Tamura, K.; Takeshita, K.; Matsushita, T. *J. Electroanal. Chem.* **1997**, *429*, 12.

(51) Gatos, H. C.; Lavine, M. C. *J. Electrochem. Soc.* **1960**, *107*, 427.

(52) Gatos, H. C.; Lavine, M. C. *J. Electrochem. Soc.* **1960**, *107*, 433.

(53) Van Muylder, J.; Pourbaix, M. In *Atlas d'Équilibres Électrochimiques*; Pourbaix, M., Ed; Gauthier-Villars: Paris, 1963.

(54) Vanleugenhaghe, C.; de Zoubov, N.; Pourbaix, M. In *Atlas d'Équilibres Électrochimiques*; Pourbaix, M., Ed.; Gauthier-Villars: Paris, 1963.

(55) Batchelor, R. A.; Hamnett, A.; Peat, R.; Peter, L. M. *J. Appl. Phys.* **1991**, *70*, 266.

(56) Solomun, T.; McIntyre, R.; Richtering, W.; Gerischer, H. *Surf. Sci.* **1986**, *169*, 414.

(57) Woodall, J. M.; Oelhafen, P.; Jackson, T. N.; Freeouf, J. L.; Pettit, G. D. *J. Vac. Sci. Technol. B* **1983**, *1*, 795.

(58) Lingier, S.; Gomes, W. P. *Ber. Bunsen-Ges. Phys. Chem.* **1991**, *95*, 170.

(59) Frese, K. W., Jr.; Morrison, S. R. *Appl. Surf. Sci.* **1981**, *8*, 266.

(60) Doligue, R. In *Nouveau Traité de Chimie Minérale*; Pascal, P., Ed.; Masson: Paris, 1958; Vol. 11, p 59.

(61) Chang, C. C.; Citrin, P. H.; Schwartz, B. *J. Vac. Sci. Technol.* **1977**, *14*, 943.

(62) Lu, Z. H.; Lagarde, C.; Sacher, E.; Currie, J. F.; Yelon, A. *J. Vac. Sci. Technol. A* **1989**, *7*, 646.

(63) Hsieh, H. F.; Shih, H. C. *J. Electrochem. Soc.* **1991**, *138*, 1965.

(64) Gerischer, H.; Hoffmann-Pérez, M.; Mindt, W. *Ber. Bunsen-Ges. Phys. Chem.* **1965**, *69*, 130.

(65) Laflère, W. H.; Cardon, F.; Gomes, W. P. *Surf. Sci.* **1974**, *44*, 541.

(66) Horowitz, G.; Allongue, P.; Cachet, H. *J. Electrochem. Soc.* **1984**, *131*, 2563.

(67) Benard, D. J.; Handler, P. *Surf. Sci.* **1973**, *40*, 141.

(68) Morrison, S. R. *Electrochemistry at Oxidized Metal Electrodes*; Plenum: New York, 1980.

(69) Lohmann, F. *Ber. Bunsen-Ges. Phys. Chem.* **1966**, *70*, 428.

(70) Gomes, W. P.; Cardon, F. *Prog. in Surf. Sci.* **1982**, *12*, 155.

(71) Lincot, D.; Vedel, J. *J. Electroanal. Chem.* **1987**, *220*, 179.

(72) Lincot, D.; Vedel, J. *J. Phys. Chem.* **1988**, *92*, 4103.

(73) Memming, R.; Neumann, G. *J. Electroanal. Chem.* **1969**, *21*, 295.

(74) Maroun, F.; Ozanam, F.; Chazalviel, J.-N. To be published.

(75) Vanmaekelbergh, D.; Gomes, W. P. *J. Phys. Chem.* **1990**, *94*, 1571.

(76) Allongue, P. In *Modern Aspects of Electrochemistry*, Vol. 23; Conway, B. E., Bockris, J. O'M., White, R. E., Eds.; Plenum: New York, 1992; Chapter 4.

(77) Crowell, C. R. *Solid-State Electron.* **1965**, *8*, 395.

(78) Nozik, A. J.; Memming, R. *J. Phys. Chem.* **1996**, *100*, 13061.

(79) Vanmaekelbergh, D. *Electrochim. Acta* **1997**, *42*, 1121.

(80) Vanmaekelbergh, D. *Electrochim. Acta* **1997**, *42*, 1135.

(81) Li, J.; Peat, R.; Peter, L. M. *J. Electroanal. Chem.* **1986**, *200*, 333.
(82) Frumkin, A. *Z. Phys. Chem.* **1925**, *116*, 466.
(83) Bard, A. J.; Faulkner, L. R. *Electrochemical Methods—Fundamentals and Applications*; Wiley: New York, 1980.
(84) Memming, R.; Neumann, G. *Surf. Sci.* **1968**, *10*, 1.
(85) Memming, R.; Neumann, G. *J. Electroanal. Chem.* **1969**, *21*, 295.
(86) Tuck, B. *J. Mater. Sci.* **1975**, *10*, 321.
(87) Kern, W. *RCA Rev.* **1978**, *39*, 278.
(88) Koper, M. T. M.; Meulenkamp, E. A.; Vanmaekelbergh, D. *J. Phys. Chem.* **1993**, *97*, 7337.
(89) Koper, M. T. M.; Vanmaekelbergh, D. *J. Phys. Chem.* **1995**, *99*, 3687.
(90) Erné, B. H.; Stchakovsky, M.; Vanmaekelbergh, D.; Ozanam, F.; Chazalviel, J.-N. To be published.
(91) Lingier, S.; Gomes, W. P.; Cardon, F. *Ber. Bunsen-Ges. Phys. Chem.* **1989**, *93*, 2.